JOURNAL OF AIRCRAFT
Vol. 45, No. 5, September–October 2008

Evolutionary-Based Multidisciplinary Design Exploration for the Silent Supersonic Technology Demonstrator Wing

Kazuhisa Chiba,* Yoshikazu Makino,† and Takeshi Takatoya‡
Japan Aerospace Exploration Agency, Tokyo 182-8522, Japan

DOI: 10.2514/1.33272

Multidisciplinary design exploration with multiple objectives was performed for the wing shape of a silent supersonic technology demonstrator, considering aerodynamics, structures, and boom noise. Aerodynamic evaluation was carried out by solving Euler equations with computational fluid dynamics, and composite structural evaluation was performed by using Nastran for strength and vibration requirements with computational structural dynamics. The intensity of the sonic boom was evaluated by a modified linear theory. The optimization problem had five objective functions: minimization of the pressure and friction drags, boom intensity at the supersonic condition, and composite structural weight and maximization of the lift at the subsonic low-speed condition. The three-dimensional wing shape defined by 58 design variables was optimized with multi-objective particle swarm optimization and an adaptive-range multi-objective hybrid genetic algorithm method. In the structural evaluation, the combination optimization of stacking sequences of laminated composites was performed for inboard and outboard wings with strength and vibration requirements. Consequently, 75 nondominated solutions were efficiently obtained through 12 generations. Moreover, data mining was performed to obtain the design knowledge for deciding a compromise solution. The data mining revealed useful knowledge in the design space, such as the tradeoff information among the objective functions and the correlations between the objective functions and design variables. A compromise solution was successfully determined by using the obtained physical design knowledge.

Nomenclature

AR	=	aspect ratio
b	=	full span length, m
C_{D_f}	=	friction drag coefficient
C_{D_p}	=	pressure drag coefficient
C_f	=	friction coefficient
C_L	=	lift coefficient
C_p	=	pressure coefficient
c_{root}, c_{kink}, c_{tip}	=	chord length at the root, kink, and tip positions, m
dv1, dv2	=	design variable 1, design variable 2, etc.
$\hat{f}$	=	estimated value of unknown function f
I_{boom}	=	intensity of sonic boom, psf
M	=	Mach number
n	=	number of symmetrical stacking of laminated composites
N^{ply}	=	number of plies
Re	=	Reynolds number
S	=	reference area of the one-sided wing, m^2
S_{wet}	=	wetted area of the one-sided wing, m^2
W_c	=	composite structural weight, kg
x, y, z	=	nondimensionalized spatial coordinates
x_{normal}, y_{normal}, z_{normal}	=	normal vectors
α	=	angle of attack, deg
ΔP	=	peak value of the sonic-boom signature across the boom carpet, psf
θ	=	fiber angle of a ply, deg

Presented as Paper 2007-4167 at the 25th AIAA Applied Aerodynamics Conference, Miami, FL, 25–28 June 2007; received 5 July 2007; revision received 5 November 2007; accepted for publication 22 November 2007.

*Project Researcher, Aviation Program Group. Member AIAA.
†Senior Researcher, Aviation Program Group. Senior Member AIAA.
‡Senior Researcher, Aviation Program Group.

I. Introduction

SINCE the flight experiment of the nonpowered supersonic experimental scaled airplane NEXST-1 was succeeded in October 2005 [1], the silent supersonic technology demonstrator S^{3}TD has been researched and developed as the next step by the Japan Aerospace Exploration Agency (JAXA) [2]. The initial zeroth shape of S^{3}TD was already designed to focus on low boom and low drag. However, its shape has insufficient performance regarding lift at low speed. Therefore, the second shape with a primary purpose of lift-performance improvement would be redesigned to keep the low-boom intensity (the first shape was for a minor change to redesign the low-boom geometry). One of the focuses of this demonstrator was created using the multidisciplinary design optimization (MDO) system, because its efficient design made the best use of the computer technology.

In previous multi-objective (MO) aerodynamic optimization for a supersonic transport (SST) [3,4], a wing with a large sweepback angle and aspect ratio was generated to reduce the drag and boom intensity and to maintain the lift. However, the results did not appear to be practically manufacturable, because no consideration was given to structures. No matter how a single disciplinary optimization is performed, there is insufficient knowledge to make use of a practical design. That is, multidisciplinary design optimization is needed to design and develop a practical aircraft using a computational technique. Baker et al. [5] and Cox et al. [6] have been studying MDO for integrated aerodynamic–structural aircraft design space exploration. Recently, their research has been on the MDO regarding a high-speed civil transport with noise constraints.

Because a real-world MO problem has tradeoffs as an optimum set (hereafter referred to as *nondominated solutions*), an MO optimization should be performed to efficiently identify such tradeoffs. MO evolutionary algorithms were applied to MO optimizations to sample multiple nondominated solutions because evolutionary algorithms sought optimum solutions in parallel using a population of design candidates. In this study, the hybrid method between MO particle swarm optimization (PSO) and adaptive-range MO genetic algorithm (GA) (ARMOGA) was applied to a large-scale and real-world problem to efficiently search both global and local optimum solutions.

Moreover, the design knowledge is acquired from the MO optimization result by performing data mining. Data mining is a role

of the postprocess for MO optimization and is essential for solving the MO optimization [7]. Although design optimization problems are important for engineering, the most important point is the extraction of the design knowledge acquired by optimization results. The result obtained by the MO optimization problem using evolutionary algorithms is not the sole solution, but an optimum set, because of tradeoffs; that is, the MO optimization result provides insufficient information for practical design, because designers need a conclusive shape. Therefore, data-mining techniques can be applied to efficiently obtain fruitful design knowledge. Because the combination between the optimization and data mining is a sequence process, it is called multidisciplinary design exploration (MDE) instead of MDO in the present study. Although the previous MDE was performed for a transonic regional jet aircraft [8], this MDE system had two problems: the wing planform was fixed and no composite material was considered. The jet aircraft's MDE was dominated by aerodynamics due to these problems.

The objective of the present study is to perform the practical MDE for the S^3TD airplane on a PSO/GA hybrid method [i.e., to optimize the three-dimensional wing shape for the S^3TD airplane using computational fluid dynamics (CFD) and computational structural dynamics (CSD) evaluation tools]. Especially, wing planform would be redesigned to improve lift performance at low-speed condition and also to restrain low-boom performance. Moreover, the design knowledge for S^3TD airplane is obtained by using data mining, and a compromise solution is then determined through the designers' discussion using that design knowledge.

II. Multidisciplinary Design Exploration

The MDO problem was defined in consideration of the sequence of the projecting flight experiment. The demonstrator takes off and climbs up to an altitude of roughly 12 to 16 km at a Mach number of 0.8. After accelerating to a Mach number of 1.2 to 1.6, supersonic flight at a variety of flight conditions is performed for approximately 5 min to measure the sonic boom on the ground and in the air. The noise measurements are also taken under takeoff and landing conditions. Flight time is roughly 17 min. The details of the background of the present S^3TD project and the conceptual design of the initial zeroth shape as the reference configuration in this study are shown in [2].

Figure 1 shows the flowchart of the present MDE system. The design problems were first defined (objective functions, constraints, and design space), optimization was next performed to obtain nondominated solutions, then a database was constructed. When nondominated solutions are lopsidedly in the design space, the response surface method is frequently used to regulate the location of solutions. In this study, the obtained nondominated solutions were directly employed as the design database. For the generated design database, data mining was performed to extract design knowledge such as tradeoffs and the correlation among objective functions, characteristic performances, and design variables.

A. Objective Functions

The following five objective functions were defined. The first three objective functions are for aerodynamics, the fourth is for noise, and the last is for structures:

1) Minimize the pressure drag at the supersonic cruising condition $S \cdot C_{D_p}$ (Mach number of 1.6, altitude of 16 km, and target C_L of 0.132 for the reference configuration of S^3TD. $S \cdot C_L^{\text{supersonic}} = \text{const}$, where S denotes the one-sided wing reference area).

2) Minimize the friction drag at the supersonic condition $S \cdot C_{D_f}$. In this study, because a simple equation was used for C_{D_f} evaluation, the fidelity of each C_{D_p} and C_{D_f} was different. Therefore, the objective functions were separated to avoid the elimination of one influence.

3) Maximize the lift at the subsonic condition $S \cdot C_L$ (Mach number of 0.2 and angle of attack of 10.0 deg).

4) Minimize the sonic-boom intensity I_{boom} at the supersonic condition. This objective-function value was defined as $|\Delta P_{\max}| + |\Delta P_{\min}|$ at the location with the largest peak of sonic-boom signature across the boom carpet.

5) Minimize a composite structural weight W_c with the fulfillment of the strength and vibration requirements. The design variables were defined by using a fiber angle of ply and a number of ply. When an individual could not be satisfied with the requirements, the penalty was given to the rank in the optimizer.

There was expected to be a tradeoff between $S \cdot C_{D_p}$ and W_c as well as between $S \cdot C_{D_p}$ and $S \cdot C_L$. Therefore, there was no constraint regarding the objective functions.

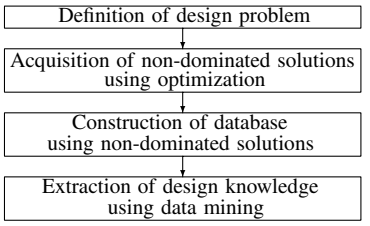

Fig. 1 Flowchart of the present multidisciplinary design exploration.

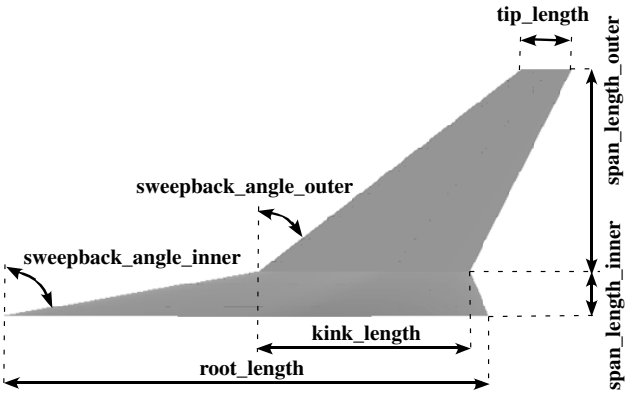

Fig. 2 Wing planform definition using seven design variables.

B. Geometry Definition

The design variables were related to planform, airfoil shape, wing twist, and position relative to the fixed fuselage on the reference configuration. Because the reference configuration of the fuselage was carried out with a low-boom and low-drag design, the fuselage was fixed. A wing planform with a kink was determined by seven design variables, as shown in Fig. 2. Airfoil shapes were defined at the wing root, kink, and tip using thickness distributions and camber lines. The thickness distributions were described by Bézier curves using nine control points with 10 design variables and were linearly interpolated in the spanwise direction. The camber-line distributions were parameterized using Bézier curves with four control points with four design variables and were incorporated linearly in the spanwise direction. Wing twist was represented by using B-splines using six control points with six design variables. The twist position was 80% chordwise location so that the straight hinge line for the aileron was secured. The position of the wing root relative to the fuselage was parameterized by the z coordinates of the leading edge, angle of attack, and dihedral. The entire computational geometry was thus defined by using 58 design variables, summarized in Table 1. Although the S^3TD has the components of fuselage, main wing, engine, and tail wing, the wing–body configuration was considered, as shown in Fig. 3. In the present study, a robust surface mesh was automatically generated in the following steps: a) generation of the wing geometry, b) extraction of the intersection line between the body and wing, c) deletion of the wing geometry (which is inside the body, and they are united), d) generation of the mesh point distributions along created ridges, and e) generation of unstructured surface mesh using the advancing-front method [9].

Table 1 Detail of design variables

Serial number	Correspondent design variable	
1, 2	Span length	Inboard, outboard
3–5	Chord length	Root, kink, tip
6, 7	Sweepback angle	Inboard, outboard
8	z coordinate	Root leading edge
9	Angle of attack for attachment to fuselage	
10	Dihedral angle	
11–22	Camber control points	Root, kink, tip
23–52	Thickness control points	Root, kink, tip
53–58	Twist control points	

C. Constraints

The geometrical constraints were considered for wing shape definition. The ridge line between the wing and fuselage should be extracted. Moreover, the chord length c should satisfy $c_{\text{root}} > c_{\text{kink}} > c_{\text{tip}}$. In addition, the constraint of maximum thickness at each spanwise location was considered. When an individual corresponded to a constraint, another individual was generated because the individual could not take form as an airplane. This operation was run repeatedly until the provided population size was set. In addition, there was no geometrical constraint regarding wing volume, because it was indirectly estimated in the evaluation of the sonic-boom intensity using equivalent area distribution.

In this study, there was no constraint for the objective functions because they were selected to give tradeoffs. For this reason, the aerodynamic evaluation was performed for all configurations with and without the satisfaction of the structural requirements. This operation might be loss of the computational cost for aerodynamic evaluations. However, the optimum wing shape for aerodynamics and sonic-boom noise might have a large sweepback angle and a large aspect ratio. Therefore, more a practical geometry can be explored to simultaneously optimize aerodynamics, sonic-boom noise, and structures.

D. Optimizer

A hybrid method between PSO [10,11] and GA [12,13] was employed. Recent optimization work often uses a response surface model (RSM) based on a kriging surrogate model to restrain evaluation time [14–16]. However, when an optimization problem with many design variables is considered, many initial sample points are needed to maintain the accuracy of the response surface [17]. In the present study, RSM is not selected, to avoid the long evaluation time for many initial samples. In addition, because the designers are required to present many optimum solutions for the decision of a compromise solution, an evolutionary-based Pareto approach was employed as an efficient multithread algorithm, instead of a gradient-based method.

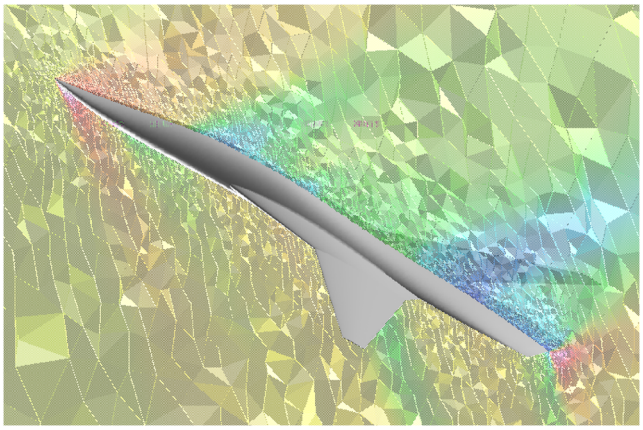

Fig. 3 The zeroth shape as the reference configuration without engine and tail wing on unstructured mesh shaded by the pressure distribution.

GAs generally do not have the capability to search for local optima, but they are able to perform a global search. On the other hand, PSO can efficiently search for local optima, because it deals with the coordinates of design variables directly. The hybridization between them may produce both capabilities. Because PSO and GA use mutation (called a perturbation in PSO) for the maintenance of solution diversity and the prevention of convergence to a local optima, the convergence to Pareto solutions becomes worse. The PSO/GA hybrid method improves diversity and enriches the quality of the obtained solutions. It is notable that PSO means multi-objective PSO, and GA denotes ARMOGA in this study.

The real-coded MOGA was used in this study because the value of design variables is directly employed for the chromosomes of an individual. Regarding crossover, the blended crossover method (BLX-α) [18] and the principal component analysis-BLX-α method (PCA-BLX-α) [19] were used, and then one-fourth of the population size was assigned to each crossover method. The other population was assigned to PSO. When the mutation rate is high, an evolutionary algorithm search is close to a random search and results in slow convergence. Therefore, the mutation rate was defined by using the inverse of the number of design variables in this study.

E. Evaluation Method

The present exploration system prepared two evaluation modules for aerodynamics, structures, and boom noise. Because the structures module used the result of aerodynamic evaluation, these phases were carried out one by one. The master processing element managed PSO/GA, and the slave PEs computed aerostructural evaluation processes. Slave processes did not require synchronization. It took roughly seven days to evaluate one generation. It is notable that the accuracy of each evaluation tool for aerodynamics, structures, and boom noise was validated through the NEXST-1 design [20,21] and the conceptual design of the S^{3}TD reference configuration [22].

1. *Aerodynamic Evaluation*

In the present study, the TAS code, a parallelized unstructured Euler/Navier–Stokes solver using domain decompositions and a message-passing-interface library, was employed to evaluate $S \cdot C_{D_p}$ and $S \cdot C_L$. The three-dimensional Euler equations were solved with a finite volume cell-vertex scheme on the unstructured mesh [9]. The Harten–Lax–van-Leer–Einfeldt–Wada Riemann solver [23] was used for the numerical flux computations. Venkatakrishnan's limiter [24] was applied when reconstructing the second-order accuracy. The lower-upper symmetric-Gauss–Seidel implicit scheme [25] was applied for time integration.

Euler computations were performed under subsonic and supersonic flight conditions, respectively. Taking advantage of the parallel search in PSO/GA, the present optimization was parallelized. Moreover, the CFD computation was also parallelized on the scalar machine.

The following Prandtl–Hoerner equation was used for the estimation of $S \cdot C_{D_f}$ to avoid huge computational time due to Navier–Stokes computation. This empirical equation is often employed for practical designs in business:

$$C_{D_f} = C_f(Re, M) \cdot \frac{S_{\text{wet}}}{S} = \frac{0.455}{(\log_{10} Re)^{2.58}} \cdot (1 + 0.15M^2)^{-0.58} \cdot \frac{S_{\text{wet}}}{S} \tag{1}$$

2. Structural Evaluation

In the present MDE system, structural optimization of wing stacking sequences of laminated composites was performed to realize minimum W_c with constraints of strength and vibration requirements. The vibration requirement was defined instead of the flutter requirement. Given the wing outer mold line for each individual, a finite element model was automatically generated from the aerodynamic evaluation results of the supersonic cruising condition, such as the coordinates, pressure coefficient, and normal vector (x, y, z, C_p, x_{normal}, y_{normal}, and z_{normal}), shown in Fig. 4. The strength and vibration characteristics were evaluated by using the commercial software MSC Nastran. The wing had inner and outer boards. The inboard wing was composed of multiframe structures (frame, rib, and spar). The outboard wing was compounded from a full-depth honeycomb sandwich structure.

There were six design variables: the stacking sequences (fiber angle of a ply θ and number of symmetrical stacking n) of the skin in the outboard wing, the skin in the inboard wing, and the frames in the inner wing; θ was defined as having symmetrical stacking $[0/\theta/-\theta/90]_{ns}$. It is notable that n was set to $^{\forall}n \in \boldsymbol{N} \leq 25$. When n was greater than 25, the individual could not fulfill the structural requirements. A rank has penalty in the optimizer. Note that θ was set to 15, 30, 45, 60, and 75 deg. Because the stacking-sequence optimization is performed for three parts (the skin in the outer wing, the skin in the inner wing, and the frames in the inner wing), the combination case is 5^3 for one individual. Nastran evaluation is repeated for one individual with 5^3 combination cases until the structural requirements are satisfied.

First, strength analysis was carried out until six design variables fulfilled the strength requirement at each node of finite element model mesh on each stacking sequence. Then vibration analysis was performed using the combinations of the design variables satisfied with the strength requirement until they fulfilled the vibration requirements (greater than 8 Hz for bending-first mode and greater than 50 Hz for twist-first mode). The computational condition was set to the symmetrical maneuver $+6$ g and the margin of safety was set to 1.25. The speed of sound and the air density was set under the condition of altitude of 16 km.

3. Sonic-Boom Evaluation

The computer-aided design (CAD)-based Automatic Panel Analysis System (CAPAS) [22] was used to evaluate I_{boom}. CAPAS was a conceptual aerodynamic design tool at JAXA. This tool comprised four design processes, as follows: 1) the geometry definition of the airplane component, 2) a combination of all components in an airplane configuration using an application program interface for CATIA V4, 3) the generation of panel and aerodynamic analyses using the panel method, and 4) a sonic-boom analysis using a modified linear theory. An aerodynamic evaluation module in CAPAS was low fidelity, because the geometry was inaccurate due to the rough computational panel, and so the aerodynamic performance in CAPAS was used only to evaluate I_{boom}.

F. Data Mining

Although a design optimization is important for engineering, the most significant point is the extraction of the knowledge in design space. The results obtained by MO optimization are not a sole solution, but an optimum set. That is, multi-objective optimization result is insufficient information for practical design, because

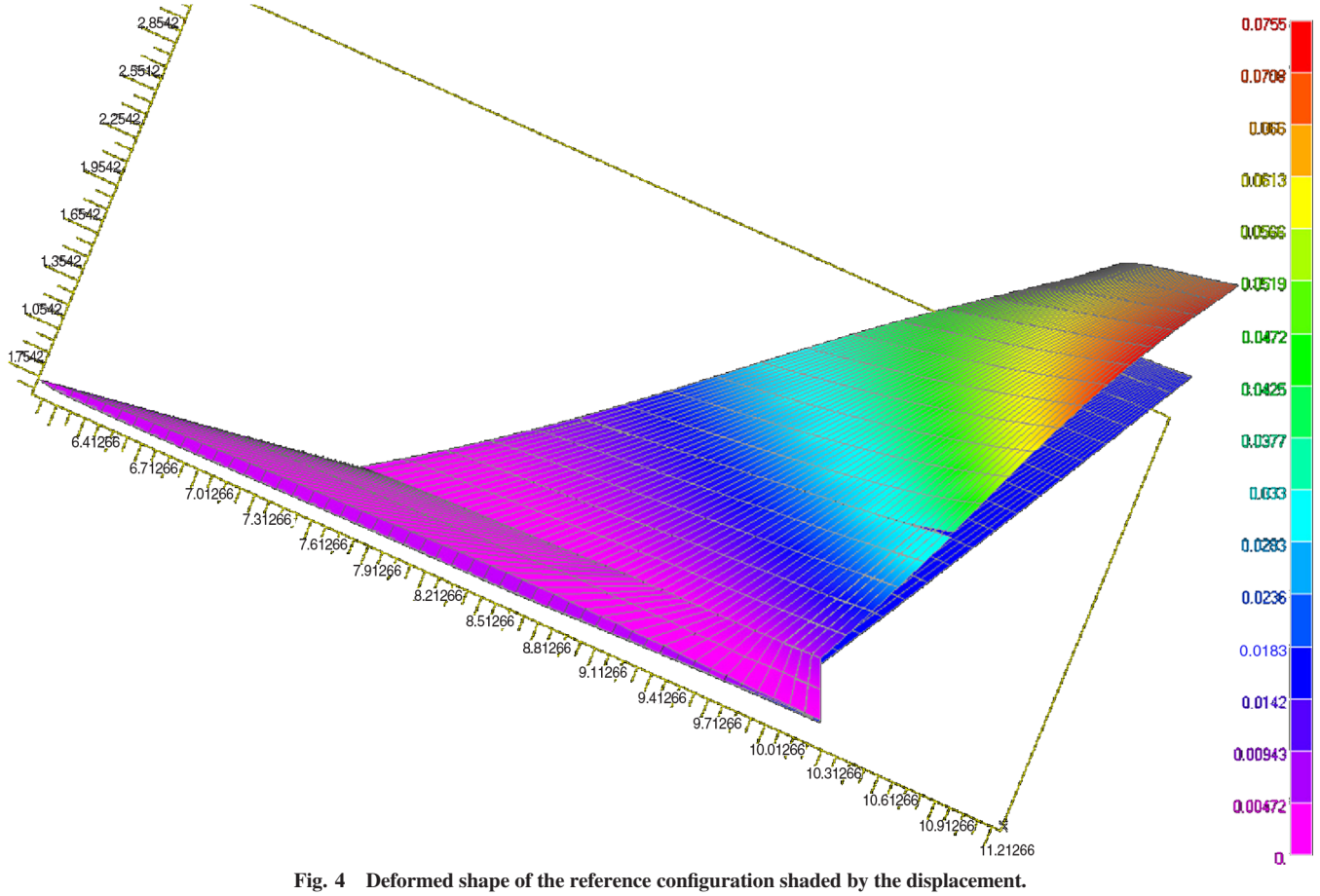

Fig. 4 Deformed shape of the reference configuration shaded by the displacement.

designers need a conclusive shape. However, the result of MO optimization can be used as a hypothetical design database. Data mining as a postprocess for optimization is essential to efficiently obtain fruitful design knowledge [26,27]. In the present study, functional analysis of variance (ANOVA) [28,29] and a self-organizing map [30] (SOM) were used for the data-mining technique. The distinguishing feature of a self-organizing map is the generation of a qualitative description. The advantage of this method includes the intuitive visualization of two-dimensional shaded maps of design space using bird's-eye-like views. As a result, SOM directly reveals the tradeoffs among objective functions. Moreover, SOMs roughly address the effective design variables and also reveal how a specific design variable affects objective functions and other design characteristics. However, SOM is subjective, due to shade cognizance. There is also a possibility of oversight because of a large number of objective functions and design variables. On the other hand, the distinguishing property of ANOVA is the quantitative description. The advantage of this method is the fact that it directly finds globally effective design variables. But ANOVA cannot directly identify the effects of design variables on objective functions. When two methods are combined, the results obtained can compensate for the disadvantages of the individual methods [7].

ANOVA is one of the data-mining techniques showing the effect of each design variable to the objective and the constraint functions in a quantitative manner. ANOVA uses the variance of the model due to the design variables on the approximation function. By decomposing the total variance of model into the variance due to each design variable, the influence of each design variable on the objective function can be calculated. The decomposition is accomplished by integrating the variables of model $\hat{f}$, where $\hat{f}$ denotes an estimated value of unknown function f.

On the other hand, SOM is an unsupervised-learning nonlinear projection algorithm from high- to low-dimensional space. This projection is based on self-organization of a low-dimensional array of neurons. In the projection algorithm, the weights between the input vector and the array of neurons are adjusted to represent features of the high-dimensional data on the low-dimensional map. The two close patterns are in the original space; the closer pattern is the response of two neighboring neurons in the low-dimensional space. Thus, SOM reduces the dimension of input data and preserves their features. The standard Kohonen algorithm adjusts the weight vector after each record is read and matched. In contrast, the batch SOM takes a batch of data (typically all records) and performs a collected adjustment of the weight vectors after all records have been matched. This is much like epoch learning in supervised neural networks. The batch SOM is a more robust approach, because it mediated over a large number of learning steps. In this study, SOMs are generated by using Viscovery SOMine 4.0 Plus [31]. In SOMine, the uniqueness of the map is ensured by the adoption of the batch SOM and the linear initialization for input data. Much like some other SOMs [32], SOMine creates a map in a two-dimensional hexagonal grid. Starting from numerical, multivariate data, the nodes on the grid gradually adapt to the intrinsic shape of the data distribution and can be read from the emerging map on the grid. The trained SOM is systematically converted into visual information [8,26].

III. Optimization Results

The population size was set to 16, taking the evaluation time for one individual into consideration. Although this size is insufficient for the number of design variables, due to the efficient evolution, even a small number of individuals obtains enough number of nondominated solutions for the extraction of design knowledge using data mining. It took roughly 6 h of CPU time of JAXA's supercomputer system and 20 processing elements for an Euler computation. The total evolutionary computation of 12 generations was performed, and 75 nondominated solutions were obtained. Here, the derived nondominated solutions are focused on, because a compromise solution is selected from them. The evolution might not converge yet. However, the result was satisfactory because several nondominated solutions achieved improvements over the reference configuration. Furthermore, a sufficient number of solutions was searched so that data mining of the design space could be performed. This can provide useful knowledge for designers.

Figure 5 shows the nondominated solutions projected on the two-dimensional plane between two objectives. This figure indicates the following tradeoff information: There are tradeoffs between $S \cdot C_L$ and W_c; there are especially severe tradeoffs between $S \cdot C_{D_p}$ and $S \cdot C_L$, and $S \cdot C_{D_f}$ and $S \cdot C_L$; but there is no tradeoff between $S \cdot C_{D_p}$ and $S \cdot C_{D_f}$. The relations are obscure between the other combinations of the objective functions. This figure shows that the reference configuration is one of the nondominated solutions and it is on the edge of the objective-function space, because two values of design variables to describe the reference configuration (the span length and sweepback angle of the inboard wing) are near the edge of the defined design space. Because several nondominated fronts are regrettably obscure, data mining deals with the correlations among the objectives.

A. Comparison Among the Extreme Solutions Regarding the Objective Functions

There are three extreme solutions, which means the champions for each objective, noted as nondominated solutions (NDS) A, B, and C. NDS-A denotes an individual in which $S \cdot C_{D_p}$ and I_{boom} were minimized. NDS-B is an individual in which $S \cdot C_{D_f}$ and W_c were minimized. NDS-C is an individual in which $S \cdot C_L$ was maximized. It is notable that the individuals without fulfillment of strength/vibration requirements were eliminated from the candidates. The planform shapes are shown in Fig. 6, and their geometrical characteristics are summarized in Table 2. Note that AR, $S_{\text{wing}}^{\text{wetted}}$, and N^{ply} denote the aspect ratio, wetted area of one side wing, and number of ply (for the skin of the outboard wing, the skin of the inboard wing, and the multi frames of the inboard wing), respectively; AR defines $b^2/(S \cdot 2)$, where b is a full span length. The objective-function values are also summarized in Table 3.

NDS-A shows that a large swept angle of the leading edge holds the front boom. Therefore, the minimizations of $S \cdot C_{D_p}$ and I_{boom} are achieved simultaneously. But because the eigenvalue of twist-first mode becomes low, the ply should be stacked for the skin of the inboard wing. NDS-B reveals that the smallest wing area achieves the minimization of $S \cdot C_{D_f}$, and the smallest wing area and the low swept angle of leading edge realize the minimization of W_c. But because the angle of attack at the supersonic cruising condition must be high to secure the target C_L, the separation might be triggered. Furthermore, a high landing speed must be also secured because of a small wing area. NDS-C shows that a large wing area achieves the maximization of lift at the subsonic condition. But the drags and W_c become high, due to the large wing area. The wing planforms of these solutions indicate that the wing area has strong effects on the objective functions in this study. The shapes of these extreme solutions show that the optimizer can efficiently explore to the edge of the design space. Consequently, the extreme solutions cannot design practically, and a compromise geometry would be decided using the knowledge in the design space.

IV. Data-Mining Results

Although SOM looks at the global knowledge in the design space like a bird's-eye view, it has a disadvantage in that it is possible to overlook the design knowledge due to the large number of design variables. In this study, data mining by SOM was performed after key design variables were addressed by ANOVA.

A. Knowledge Acquired by Using ANOVA

The variance of the design variables and their interactions by ANOVA are shown in Fig. 7. Their proportions are shown, which were larger than 1% to the total variance. It is notable that ANOVA was analyzed by using the data eliminated: an individual with a great value leap for I_{boom} and 16 individuals without fulfillment of

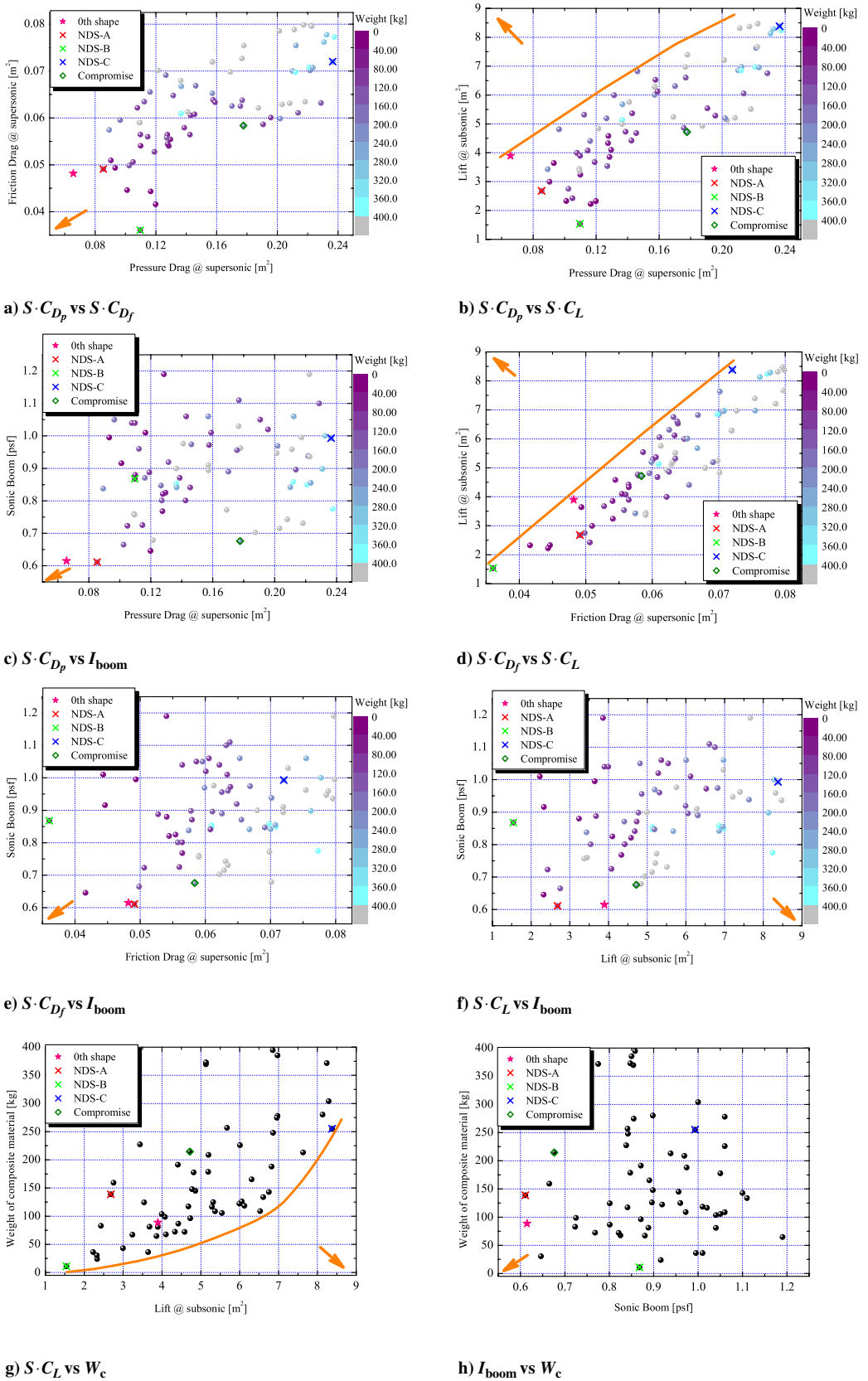

a) $S \cdot C_{D_p}$ vs $S \cdot C_{D_f}$

b) $S \cdot C_{D_p}$ vs $S \cdot C_L$

c) $S \cdot C_{D_p}$ vs I_{boom}

d) $S \cdot C_{D_f}$ vs $S \cdot C_L$

e) $S \cdot C_{D_f}$ vs I_{boom}

f) $S \cdot C_L$ vs I_{boom}

g) $S \cdot C_L$ vs W_c

h) I_{boom} vs W_c

Fig. 5 Derived nondominated solutions on two-dimensional planes between the objective functions. The arrow denotes the optimum direction and the line describes the discernible nondominated front.

structural requirements. The symbol dv denotes the design variable and - denotes the interaction between two design variables.

Figure 7a shows that dv25, dv14, dv1, and dv6 have an effect on $S \cdot C_{D_p}$; dv25 describes the leading-edge bluntness at the root. Because the wing thickness at the root is largest, due to the long chord length, the leading-edge bluntness at the root is most effective on $S \cdot C_{D_p}$. The height of the rearward camber at the root is represented by dv14, which also decides the angle that the flow takes on the

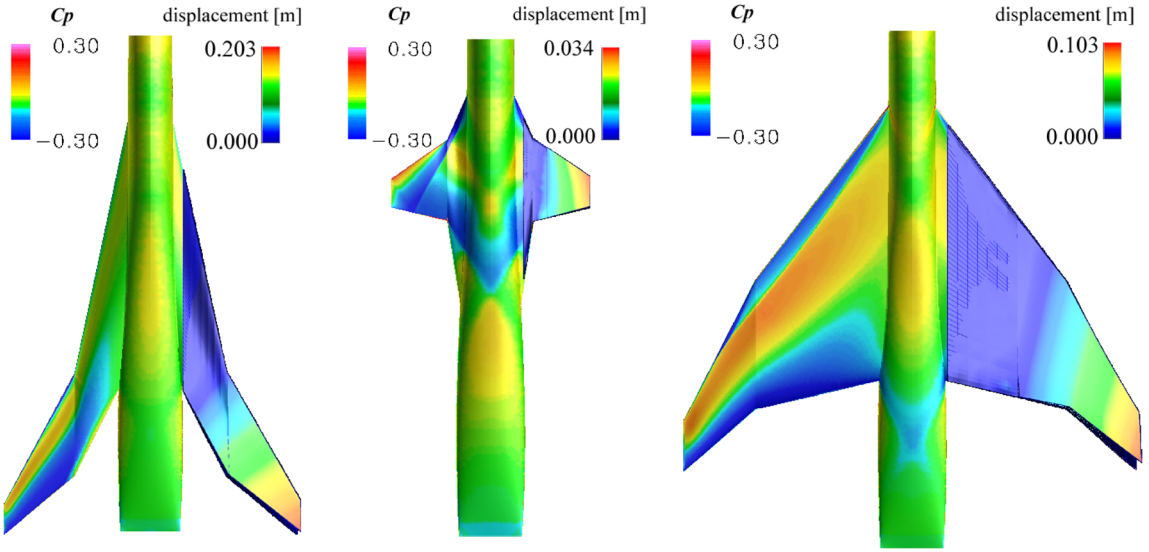

a) NDS-A **b) NDS-B** **c) NDS-C**

Fig. 6 Comparison among the wing planform of the extreme solutions shaded by C_p distribution on CFD and displacement on CSD.

rearward wing. Because the curvature of camber line becomes large when the value of dv14 becomes high, $S \cdot C_{D_p}$ increases. The inboard span length is described by dv1; because the wetted area increases when dv1 becomes high, $S \cdot C_{D_p}$ increases.

Figure 7b shows that dv1, dv2, and dv4 have an effect on $S \cdot C_{D_f}$. It reveals that the span length and the chord length at the kink are effective with $S \cdot C_{D_f}$. In this study, because the Prandtl–Hoerner equation gives $S \cdot C_{D_f}$, it becomes high when the individual has a large wetted area. Moreover, in this study, the chord length at the root does not fluctuate largely. The design variables represented by a large chord length at the kink have effects on the increase of the wing area.

Figure 7c reveals that dv1 and dv2 have effects on $S \cdot C_L$. The span length of the inboard wing decides the $S \cdot C_L$. The mechanism by which $S \cdot C_L$ increases due to the span length is similar to that of the $S \cdot C_{D_f}$ increase.

Figure 7d shows that dv6 and dv43 have effects on I_{boom}. The leading-edge sweepback angle of inner wing is described by dv6. Because the I_{boom} at the front boom becomes weak when this angle becomes large, the total of I_{boom} thus decreases.

Figure 7e shows that dv25 and dv16 have effects on W_c. The leading-edge bluntness at the root is described by dv25. Because the wing becomes thin near the leading edge when the leading edge has sharpness, the strength becomes weak and the natural frequency becomes low. Because the number of plies should increase to fulfill the structural requirements, W_c increases. The frontward camber height at the kink is described by dv16. The curvature of camber line multiplies strength and increases natural frequency. The camber height has an effect on W_c.

Table 2 Geometrical characteristic values of the extreme solutions

Individual	$C_{L\,\text{design}}$	α_{cruise}, deg	AR	$S_{\text{wing}}^{\text{wetted}}$, m^2	$N_{\text{out}_{\text{skin}}}^{\text{ply}}/N_{\text{in}_{\text{skin}}}^{\text{ply}}/N_{\text{in}_{\text{rib}}}^{\text{ply}}$
NDS-A	0.1300	3.94	2.92	10.81	16/88/32
NDS-B	0.3103	6.85	2.86	4.15	8/24/8
NDS-C	0.0632	1.76	3.08	22.52	56/48/56

B. Knowledge Acquired by Using SOM

The resulting 75 nondominated solutions were projected onto the two-dimensional map of SOM. Figure 8 shows the shaded SOM by the objective functions with 11 clusters, taking the five objective functions into consideration. Figure 8a shows that the left area collects the designs with high $S \cdot C_{D_p}$, and the right area collects the designs with low $S \cdot C_{D_p}$. Figure 8b shows that the upper left area collects the designs with high $S \cdot C_{D_f}$, and the upper right area collects the designs with low $S \cdot C_{D_f}$. Figure 8c shows a shading pattern similar to that in Fig. 8b. Figure 8d shows that the lower right area collects the designs with high I_{boom}. There is no clear pattern regarding low I_{boom}. Figure 8e shows that the upper left area collects the designs without fulfillment of the structural requirements, and the right area collects the designs with low W_c. This result is summarized in Fig. 9.

Figure 8 reveals the following tradeoff and correlation information. There is no tradeoff between $S \cdot C_{D_p}$ and $S \cdot C_{D_f}$. On the other hand, there are strong tradeoffs between $S \cdot C_L$ and $S \cdot C_{D_p}$ and between $S \cdot C_L$ and $S \cdot C_{D_f}$. There is no correlation between I_{boom} and the other objectives; that is, I_{boom} does not depend on the other objectives in the design space. In this study, there is no tradeoff between $S \cdot C_{D_p}$ and I_{boom} because the fuselage is fixed. The nose geometry is generally effective to the tradeoff between them. There is correlation among W_c and $S \cdot C_{D_p}$ and among $S \cdot C_{D_f}$ and and $S \cdot C_L$ when W_c becomes low. This tradeoff information corresponds to the knowledge shown in Fig. 5, and the intimate correlation among the objective functions is additionally revealed. Moreover, because the cluster on the upper right corner in Fig. 8 has low values for all objectives, there is a feasible tradeoff region when $S \cdot C_L$ is tolerable. But the primary objective of this MDO is to improve the lift performance at low speed. The knowledge regarding this feasible tradeoff region suggests that the other four objectives are corrupted compared with the reference configuration, even when any compromise-solution with improved lift performance at low speed is selected.

Figure 10 shows the SOMs shaded by C_{D_p} and C_L. Figure 10a shows that the upper right area collects the high C_{D_p}, and the upper

Table 3 Comparison of the objective-function and aerodynamic-performance values among the extreme solutions

Individual	$S \cdot C_{D_p}$	(C_{D_p})	$S \cdot C_{D_f}$	$S \cdot C_L$	(C_L)	I_{boom}	W_c
NDS-A	**0.0854**	(0.0152)	0.0491	2.682	(0.4765)	**0.611**	138.7578
NDS-B	0.1097	(0.0465)	**0.0361**	1.540	(0.6534)	0.868	**11.01**
NDS-C	0.2365	(0.0204)	0.0720	**8.380**	(0.7238)	0.993	255.2193

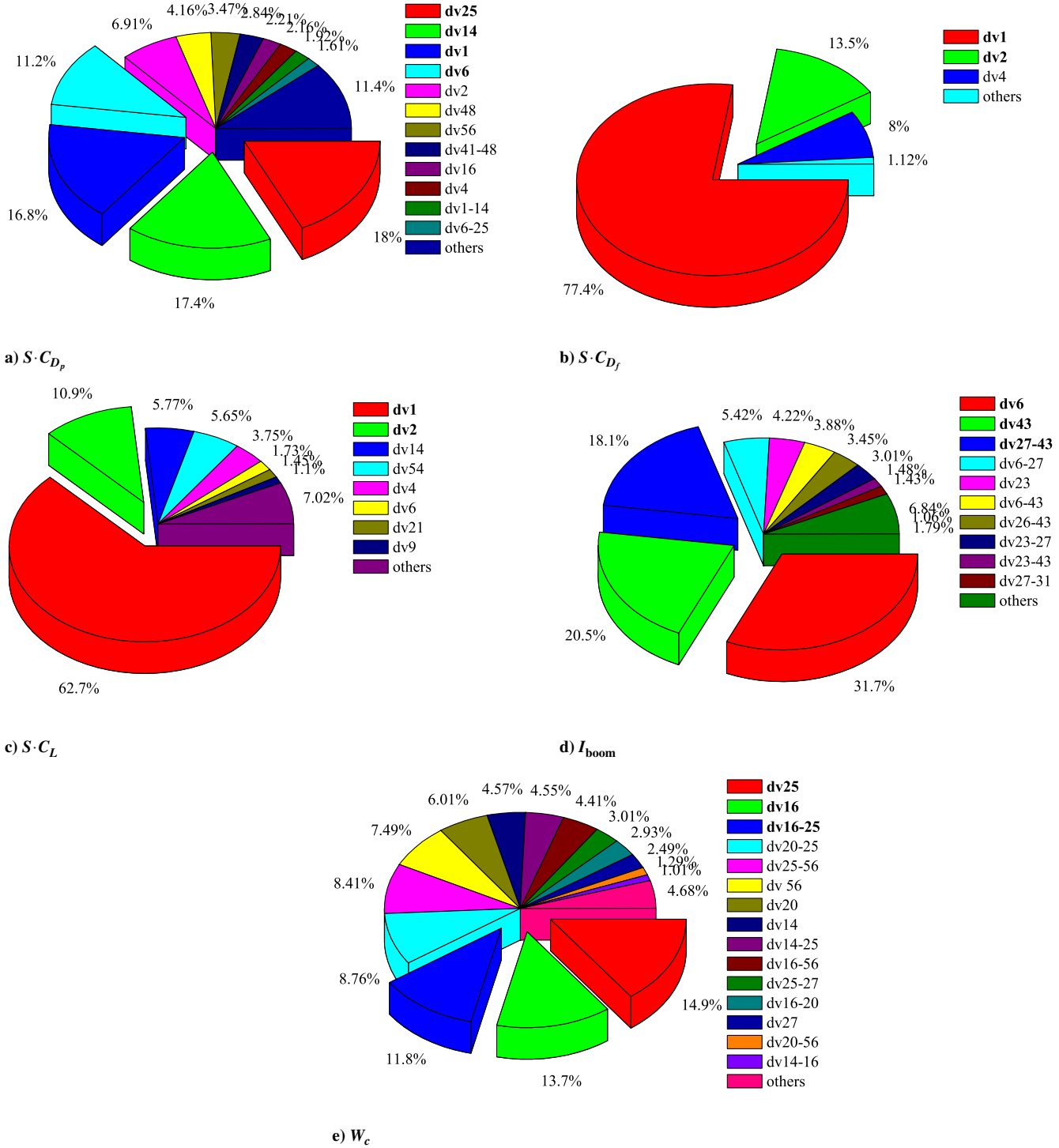

Fig. 7 Proportion of design-variable influence for the objective functions using ANOVA.

center area and lower right areas collect the low C_{D_p}. Figure 10b shows that the lower left area collects high C_L, and the right area collects low C_L; however, the shading pattern is unclear. Because the comparison among Figs. 8a, 8c, and 10 shows different shading patterns, the optimum direction disagrees between C_{D_p} and $S \cdot C_{D_p}$ and between C_L and $S \cdot C_L$. When $S \cdot C_{D_p}$ and $S \cdot C_L$ are considered, the optimum direction is dominated by the wing area.

The SOMs can be also contoured by 58 design variable values. Figure 11 shows the SOMs shaded by the characteristic design variables addressed by ANOVA. These shaded SOMs reveal how design variables operate on the objective functions. Figure 11a shows that the left area collects high dv1 and the upper right area collects low dv1. Therefore, when the span length of the inboard wing becomes high, $S \cdot C_{D_p}$, $S \cdot C_{D_f}$, and $S \cdot C_L$ become high, and when the span length of the inboard wing becomes low, $S \cdot C_{D_p}$, $S \cdot C_{D_f}$, $S \cdot C_L$, and W_c become low. Figure 11b shows that the upper left area collects high dv2. Therefore, when the span length of the outboard wing becomes high, $S \cdot C_{D_f}$, $S \cdot C_L$, and W_c become high. As Fig. 11c shows, the upper right area collects high dv6, and $S \cdot C_{D_p}$ and I_{boom} become low when the sweepback angle of the inboard wing becomes high. Figure 11d shows that left area roughly collects high dv14, but this shading pattern is insufficient to mention the correlation. Therefore, the rearward camber height at the root does not have a large effect on $S \cdot C_{D_p}$. Figure 11e shows that the upper center area collects low dv16. Therefore, W_c tends to become high

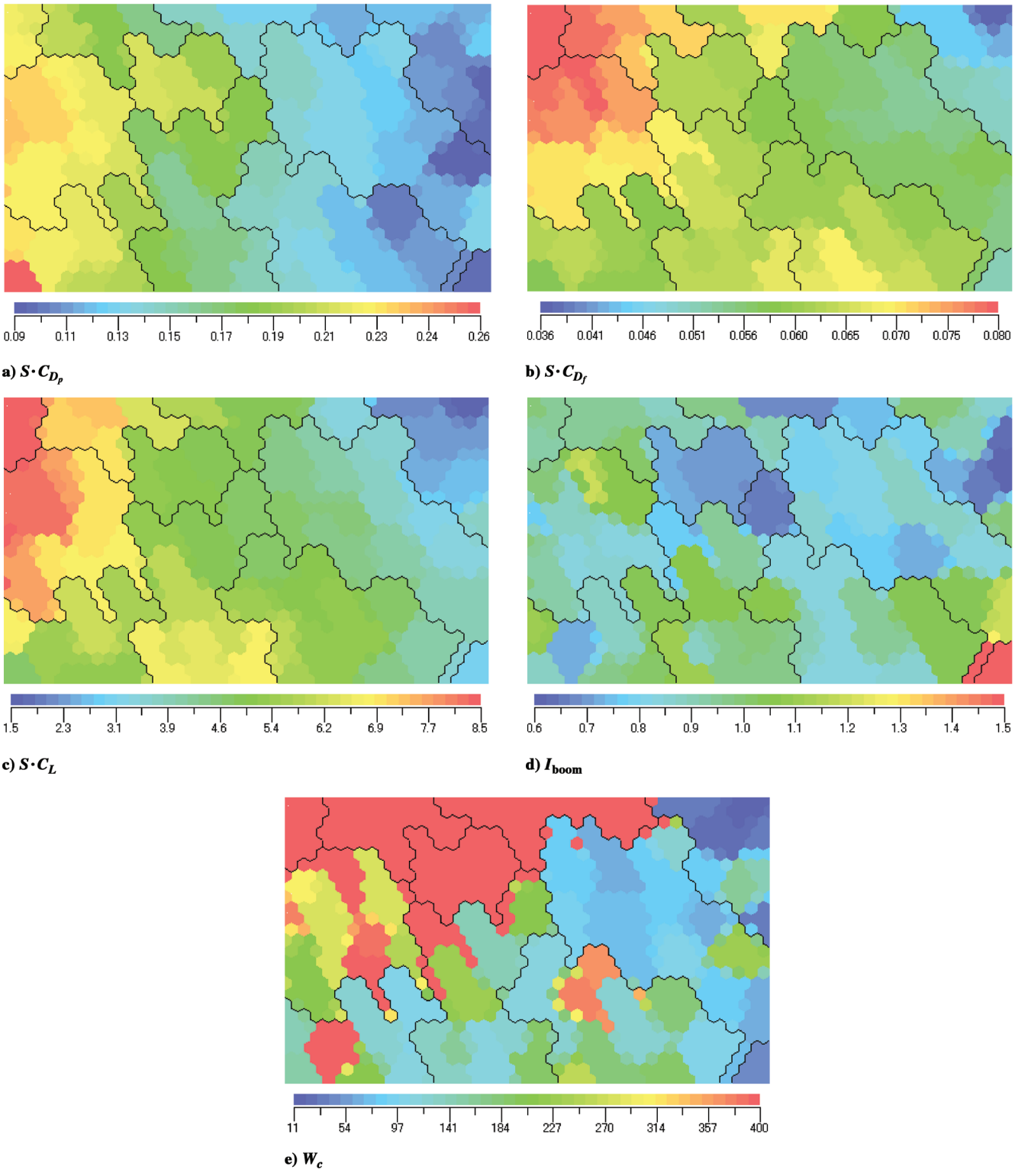

Fig. 8 SOMs shaded by the objective functions, taking the five objective functions into consideration.

when the frontward camber height at the kink becomes low. Figure 11f shows that dv25 does not fluctuate much and there is no clear contour pattern. Therefore, the leading-edge bluntness at the root does not have a large effect on the objectives. Because Fig. 11g shows that there is a, incoherent shading pattern, there is no correlation between the leading-edge bluntness at the tip and I_{boom}.

The shading patterns between two or more SOMs show the qualitative effects. SOM needs to be interpreted when the physical meaning of design variables is considered. Furthermore, the present optimization is most successful even when insufficient population and generation numbers are used, because the result of a database for data mining enrich the designers' understanding of the physical design knowledge.

C. Decision of a Compromise Solution

The 75 nondominated solutions are extracted using SOM to determine a compromise solution. The applicable solutions to the following conditions are first excluded from 75 nondominated solution:

1) The structural requirements are not fulfilled.

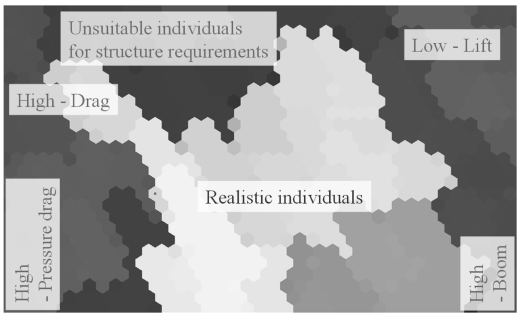

Fig. 9 SOM of the derived nondominated solutions in the five-dimensional objective-function space. Shadow region denotes that there is impractical individuals for design.

2) $S \cdot C_L$ is low or the wing area is low (this means the constraint for the landing speed).

3) $S \cdot C_{D_p}$ and $S \cdot C_{D_f}$ are impractically large.

As a result of this operation, 24 nondominated solutions emerge as the practical designs are sorted. The SOM is regenerated using the 24 derived nondominated solutions, taking the five objective functions into consideration. The derived SOM with the top views of the sorted 24 nondominated solutions and its shaded maps by the objectives are shown in Fig. 12. The compromise solution is determined from these individuals, taking the balance of the five objective functions and the low-boom competence as the primary objective of S^{3}TD into consideration on SOM. The designers clustered the similar planform shapes, and they selected the exploitable shape group as a demonstrator using the experiences that they cultivated by the development of real-world aircraft in companies. Four shapes were selected, taking the low-boom competence into consideration. Then the final compromise solution (which is improvable, due to the refinements on the fuselage and cross-sectional geometries) was ultimately determined.

D. Comparison Between the Reference Configuration and the Selected Compromise Solution

Because the compromise solution secured the wing area, low-speed aerodynamic performance could be improved and it was redesigned to have practical capability for takeoff and landing. However, because the objective functions regarding aerodynamics depended on wing area, the design knowledge about the wing cross section was insufficient.

The comparison of the planform between the reference configuration and the selected compromise solution (hereafter referred to only as *the compromise*) is shown in Fig. 13. The airfoils of reference and compromise configurations near the junction relative to the fuselage, kink, and tip are also shown. It is notable that the reference configuration has no twist and its airfoil is described as the NACA64A series. The thickness ratios are defined as 6% at the root, 5% at the kink, and 3% at the tip. The installed angle of wing is −0.5 deg relative to the fuselage. The characteristics and performance are summarized in Tables 4 and 5. Because $S \cdot C_L$ is the maximization objective, the compromise has a larger wing area than that of the reference configuration. And the inner wing area of the compromise becomes large to secure the structural strength. The sweepback angle design is milder so that the wing area and structural strength are secured and that I_{boom} does not obtain the effect. But the chord length near the kink becomes short to achieve low W_c and $S \cdot C_{D_f}$. Therefore, the number of plies increases to augment the eigenfrequency. The compromise has the supersonic leading edge near the root to reduce the effect on I_{boom} of the front boom. Also, the compromise has the blunt leading edge near the kink to improve the strength, eigenfrequency, and subsonic aerodynamic performance. Data-mining results show that the sharp leading edge near the tip has an effect on I_{boom}. But the wing area has a strong effect on the objectives. Therefore, the knowledge regarding the airfoil shape is unreliable.

The location in the design space for the reference configuration and the compromise is shown in Fig. 5. The reference configuration has low $S \cdot C_{D_p}$ and $S \cdot C_L$, due to a small wing area, and it is located on the edge in the design space. Also, it has low I_{boom}, due to focusing on low-boom design. The compromise locates the low-I_{boom} region as well as the compromise of the other objectives. The locations in Fig. 5 show that the aerodynamic performance strictly depends on the wing area. Figure 14 shows the spanwise distributions of C_L and C_D and the twist angle for the reference and compromise configurations. This figure shows that the twist angle of the compromise on the outer wing is large; that is, down lift occurs at the outboard wing. C_D becomes still larger, due to the inverted camber line near the kink. As data-mining results reveal, the design variables regarding twist and the inverted camber line have no effects on the objective functions, and the redesign of these design variables can improve the aerodynamic performance without corrupting the other objectives. The knowledge regarding the airfoil shape is insufficient. The primary reason is that its effect is weak with the aerodynamic performance compared with the wing planform. The secondary reason is that only a small number of generations were performed.

Finally, the boom intensity as the primary objective function is compared between the reference and compromise configurations. Figure 15 shows their ground pressure signatures. Although I_{boom} performance of the reference configuration is better, the

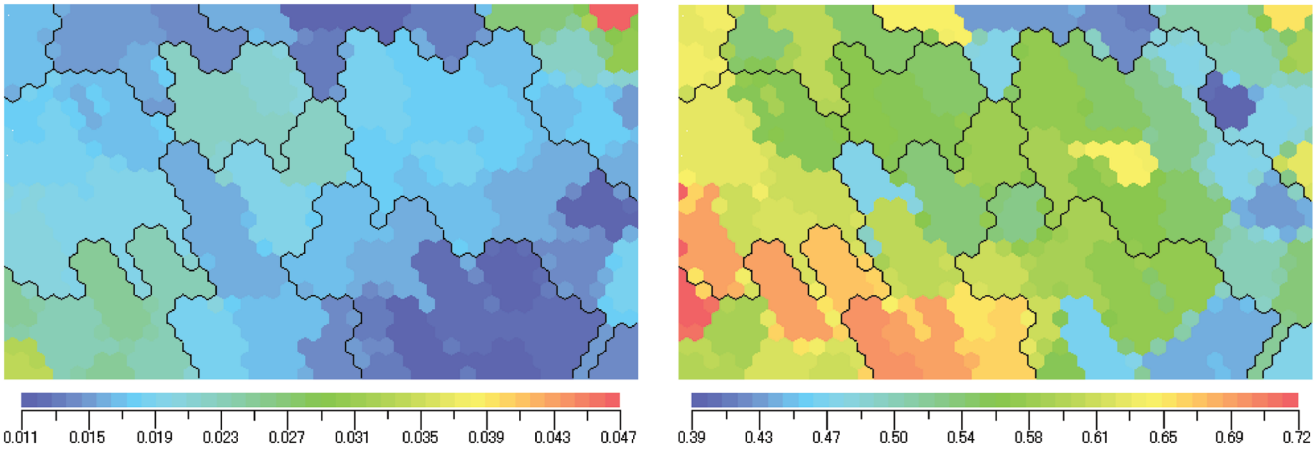

a) C_{D_p} **b) C_L**

Fig. 10 SOMs shaded by the aerodynamic characteristics.

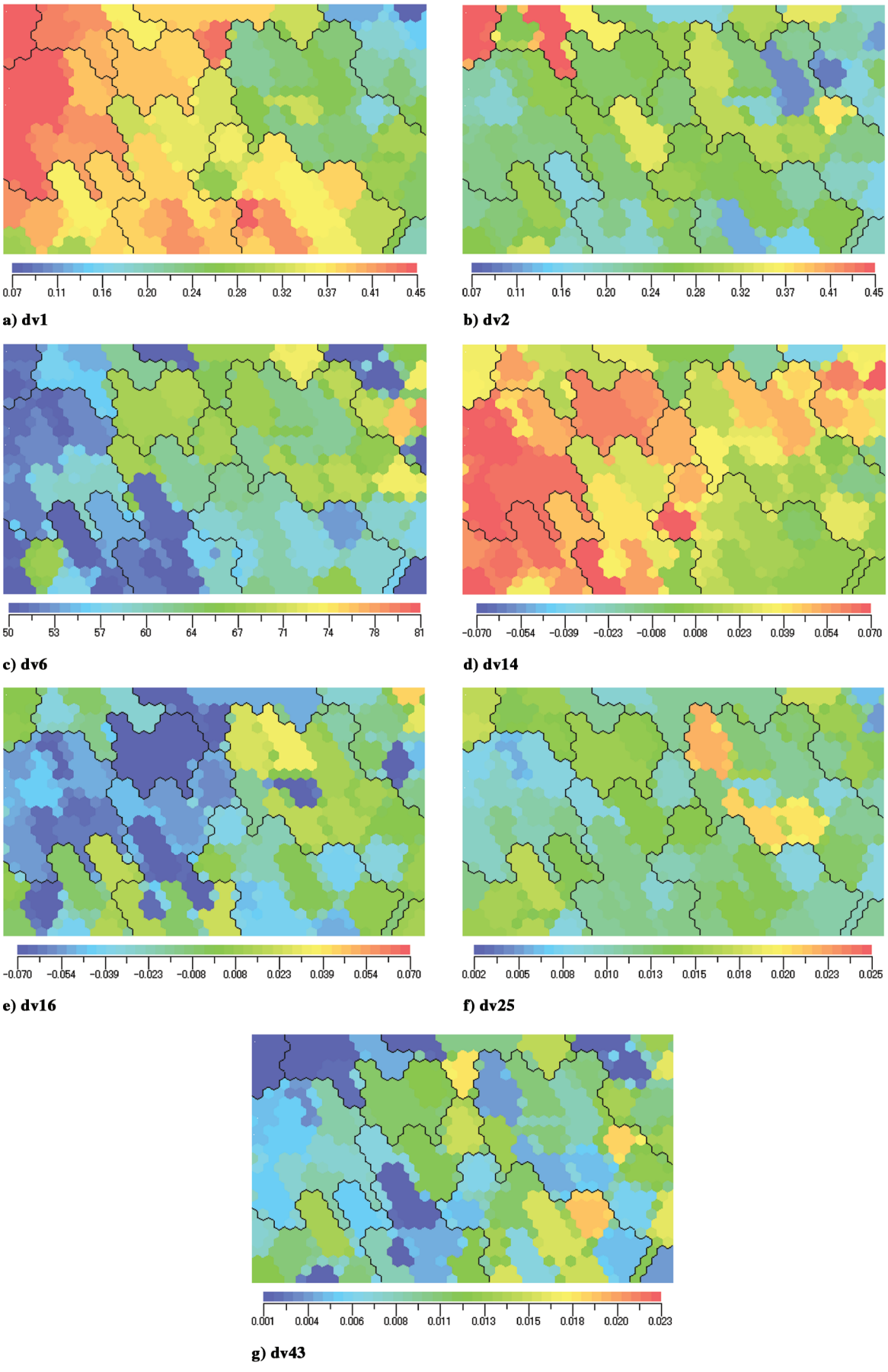

Fig. 11 SOMs shaded by the characteristic design variables indicated by ANOVA.

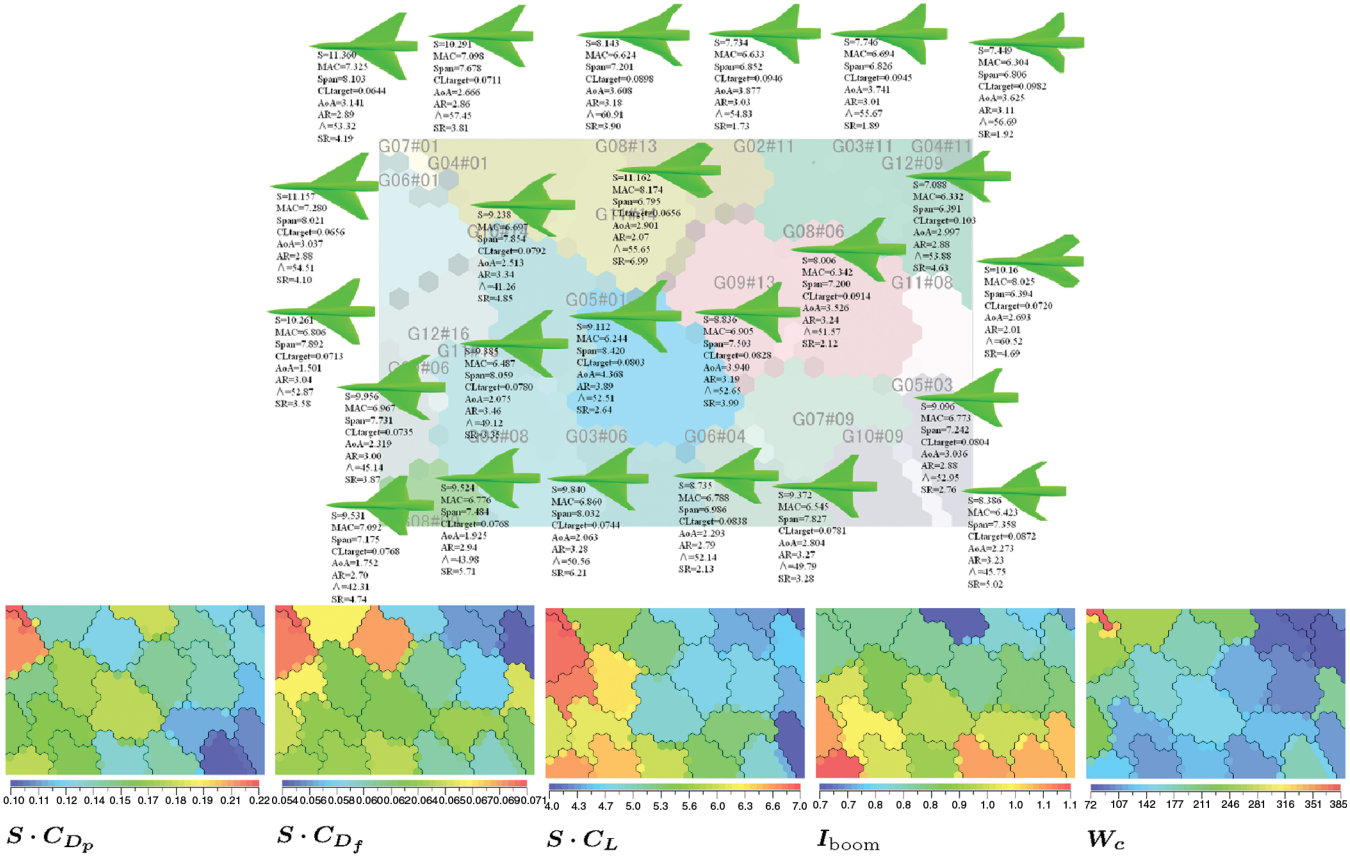

Fig. 12 Derived SOM with the top views of the sorted 24 individuals and their shaded maps by the objective functions.

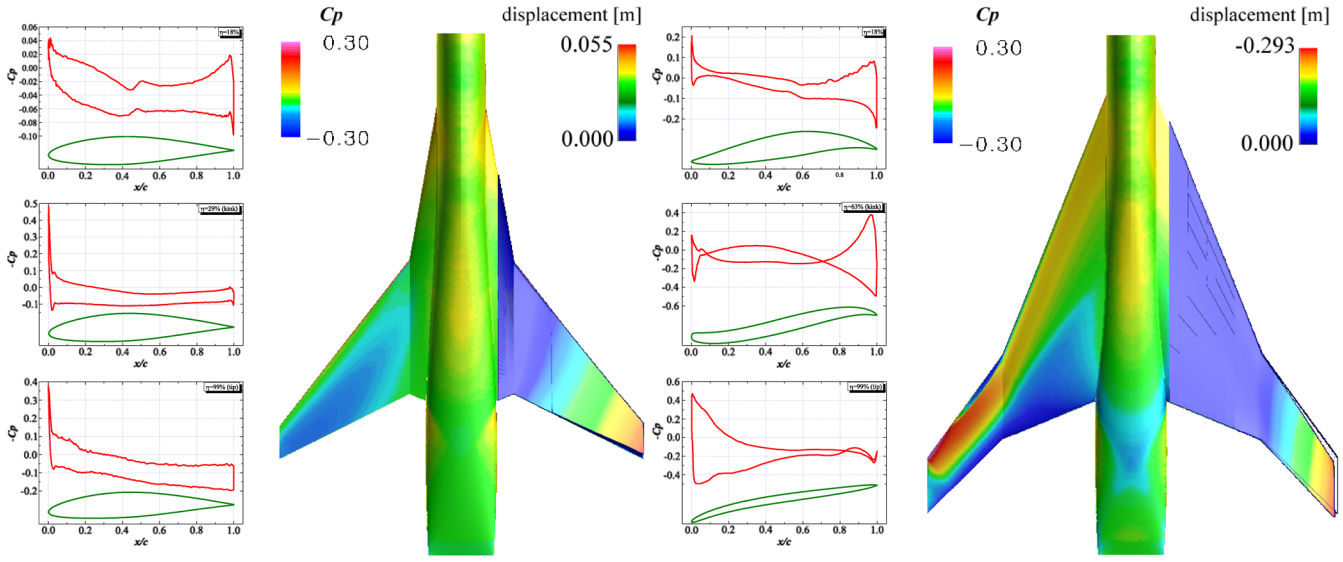

a) Reference configuration **b) Compromise solution**

Fig. 13 Comparison of wing shape shaded by C_p and displacement distributions with C_p distributions near the junction relative to the fuselage, kink, and tip.

compromise also keeps non-N-shaped signature to restrain the initial peak. The compromise has better performance of $S \cdot C_L$ for the constraint of landing speed as well as for the restraint of I_{boom}. In this study, the rearward boom intensity cannot be discussed, because the assumed fuselage-wing configuration ignores an engine nacelle and vertical/horizontal tail wings. But CFD visualization of C_p distribution on the symmetrical plane, shown in Fig. 16, reveals that a shock wave occurs in the vicinity of the wing trailing edge. It is necessary to optimize the full configuration to design the geometry-restrained rearward boom intensity and to obtain the design knowledge regarding the cross-sectional shape.

Table 4 Comparison of geometrical characteristic values between the reference configuration and the compromise solution

Individual	$C_{L\ \mathrm{design}}$	α_{cruise}, deg	AR	$S_{\mathrm{wing}}^{\mathrm{wetted}}$, m^2	$N_{\mathrm{out_{skin}}}^{\mathrm{ply}}/N_{\mathrm{in_{skin}}}^{\mathrm{ply}}/N_{\mathrm{in_{rib}}}^{\mathrm{ply}}$
Reference	0.132	2.33	3.81	10.41	8/72/24
Compromise	0.0898	3.61	3.18	15.68	56/88/24

Table 5 Comparison of the objective and aerodynamic-performance values between the reference configuration and compromise solution

Individual	$S \cdot C_{D_p}$	(C_{D_p})	$S \cdot C_{D_f}$	$S \cdot C_L$	(C_L)	I_{boom}	W_c
Reference	0.0656	(0.0118)	0.0482	3.896	(0.7029)	0.615	88.74
Compromise	0.1777	(0.0218)	0.0584	4.719	(0.5794)	0.676	214.58

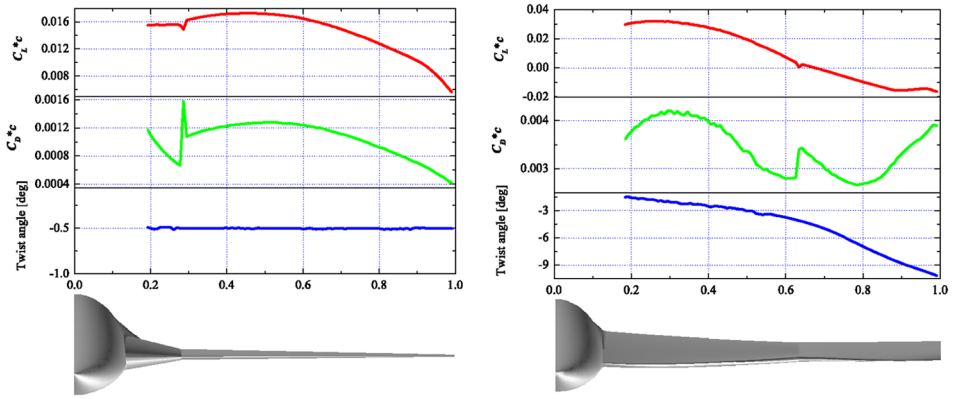

a) Reference configuration **b) Compromise solution**

Fig. 14 Comparison of the spanwise distributions of C_L and C_D with the twist angle.

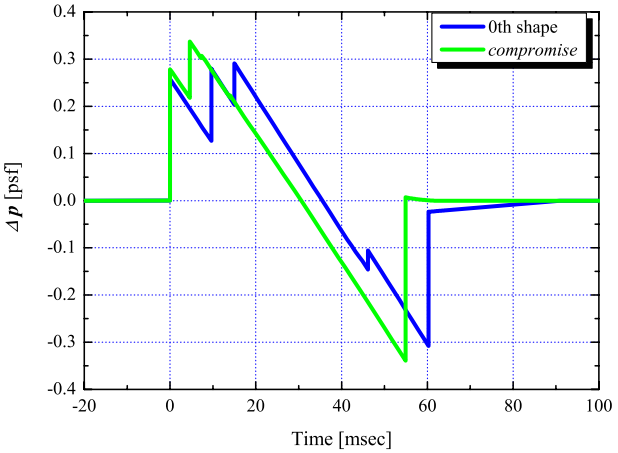

Fig. 15 Comparison of ground pressure signatures.

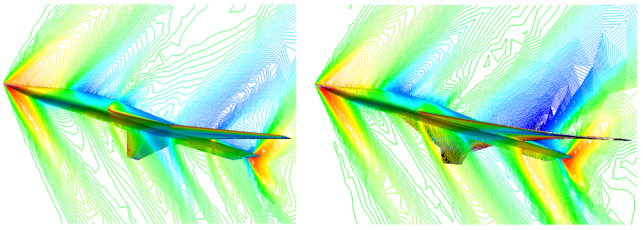

a) Reference configuration **b) Compromise solution**

Fig. 16 Comparison of pressure distributions on the symmetrical plane.

V. Conclusions

The multidisciplinary design exploration for a silent supersonic technology demonstrator wing was performed using optimization and data mining, taking five objective functions regarding aerodynamics, structures, and boom noise into consideration using multi-objective particle swarm optimization and an adaptive-range multi-objective genetic algorithm (MOGA) hybrid method. Consequently, 12 generations evolved and 75 nondominated solutions were efficiently acquired. The knowledge in the design space was obtained regarding the tradeoffs among the objective functions using data mining. Furthermore, the particular design variables that had effects on the objective functions were also revealed. The multidisciplinary design exploration system with a data-mining process was essential for a successful decision on a compromise solution. Because the compromise solution secured the wing area, low-speed aerodynamic performance could be improved, and silent supersonic technology demonstrator was redesigned to have practical capability for takeoff and landing as well as for the restraint of the intensity of the sonic boom. Because the wing area had strong effects on the objective functions regarding aerodynamics, the design knowledge about the wing cross section is insufficient. In addition, the problem turned out to be that the decided geometry could not trim. Therefore, a next-step multidisciplinary design exploration approach should be performed for the intimate configuration to redesign the cross section of the main wing and stabilizer.

Acknowledgments

We would like to thank all members of the supersonic transport team in the aviation program group at the Japan Aerospace Exploration Agency (JAXA) for providing useful advice. The Euler/

Nastran computations were performed using the Central Numerical Simulation System of the Numerical Simulator III in JAXA's Engineering Digital Innovation Center.

References

[1] Ohnuki, T., Hirako, K., and Sakata, K., "National Experimental Supersonic Transport Project," International Council of the Aeronautical Sciences Paper 2006-1.4.1, 2006.

[2] Murakami, A., "Silent Supersonic Technology Demonstration Program," Proceedings on 25th International Council of the Aeronautical Sciences, Hamburg, Germany, International Council of the Aeronautical Sciences Paper 2006-1.4.2, 2006.

[3] Alonso, J. J., Kroo, I. M., and Jameson, A., "Advanced Algorithms for Design and Optimization of Quiet Supersonic Platforms," AIAA Paper 2002-0144, 2002.

[4] Sasaki, D., Obayashi, S., and Nakahashi, K., "Navier-Stokes Optimization of Supersonic Wings with Four Objectives Using Evolutionary Algorithm," *Journal of Aircraft*, Vol. 39, No. 4, 2002, pp. 621–629.

[5] Baker, C. A., Grossman, B., Haftka, R. T., Maso, W. H., and Waston, L. T., "High-speed Civil Transport Design Space Exploration Using Aerodynamic Response Surface Approximations," *Journal of Aircraft*, Vol. 39, No. 2, 2002, pp. 215–220.

[6] Cox, S. E., Haftka, R. T., Baker, C., Grossman, B., Mason, W. H., and Waston, L. T., "A Comparison of Global Optimization Methods for the Design of a High-Speed Civil Transport," *Journal of Global Optimization*, Vol. 21, No. 4, 2001, pp. 415–432.
doi:10.1023/A:1012782825166

[7] Chiba, K., Jeong, S., Obayashi, S., and Yamamoto, K., "Knowledge Discovery in Aerodynamic Design Space for Flyback-Booster Wing Using Data Mining," AIAA Paper 2006-7992, 2006.

[8] Chiba, K., Oyama, A., Obayashi, S., Nakahashi, K., and Morino, H., "Multidisciplinary Design Optimization and Data Mining for Transonic Regional-Jet Wing," *Journal of Aircraft*, Vol. 44, No. 4, 2007, pp. 1100–1112.
doi:10.2514/1.17549

[9] Ito, Y., and Nakahashi, K., "Direct Surface Triangulation Using Stereolithography Data," *AIAA Journal*, Vol. 40, No. 3, 2002, pp. 490–496.

[10] Kennedy, J., and Eberhart, R., "Particle Swarm Optimization," *Proceedings of the Fourth IEEE International Conference on Neural Networks*, Inst. of Electrical and Electronics Engineers, Piscataway, NJ, 1995, pp. 1942–1948.

[11] Alvarez-Benitez, J. E., Everson, R. M., and Fieldsend, J. E., "A MOPSO Algorithm Based Exclusively on Pareto Dominance Concepts," *Evolutionary Multi-Criterion Optimization (EMO 2005)*, Lecture Notes in Computer Science, Vol 3410, Springer–Verlag, Berlin, 2005, pp. 459–473.

[12] Fonseca, C. M., and Fleming, P. J., "Genetic Algorithms for Multiobjective Optimization: Formulation, Discussion and Generalization," *Proceedings of the Fifth International Conference on Genetic Algorithms*, Morgan Kaufmann, San Mateo, CA, 1993, pp. 416–423.

[13] Obayashi, S., Takahashi, S., and Takeguchi, Y., "Niching and Elitist Models for MOGAs, Parallel Problem Solving from Nature," *Parallel Problem Solving from Nature (PPSN 5)*, Lecture Notes in Computer Science, Vol 1498, Springer, Berlin, 1998, pp. 260–269.

[14] Simpson, T. W., Mauery, T. M., Korte, J. J., and Mistree, F., "Kriging Models for Global Approximation in Simulation-Based Multidisciplinary Design Optimization," *AIAA Journal*, Vol. 39, No. 12, 2001, pp. 2233–2241.

[15] Keane, A. J., "Statistical Improvement Criteria for Use in Multiobjective Design Optimization," *AIAA Journal*, Vol. 44, No. 4, 2006, pp. 879–891.
doi:10.2514/1.16875

[16] Jeong, S., Murayama, M., and Yamamoto, K., "Efficient Optimization Design Method Using Kriging Model," *Journal of Aircraft*, Vol. 42, No. 2, 2005, pp. 413–420.
doi:10.2514/1.6386

[17] Keane, A. J., "Wing Optimization Using Design of Experiment, Response Surface, and Data Fusion Methods," *Journal of Aircraft*, Vol. 40, No. 4, 2003, pp. 741–750.

[18] Eshelman, L. J., and Schaffer, J. D., "Real-Coded Genetic Algorithms and Interval Schemata," *Foundations of Genetic Algorithms 2*, Morgan Kaufmann, San Mateo, CA, 1993, pp. 187–202.

[19] Takahashi, M., and Kita, H., "A Crossover Operator Using Independent Component Analysis for Real- Coded Genetic Algorithms," *IEEE Congress on Evolutionary Computation 2001*, Inst. of Elecrical and Electronics Engineers, Piscataway, NJ, 2001, pp. 643–649.

[20] Umeda, M., Takenaka, K., Hatanaka, K., Hirayama, D., Yamazaki, W., Matsushima, K., and Nakahashi, K., "Validation of CFD Capability for Supersonic Transport Analysis Using NEXST-1 Flight Test Results," AIAA Paper 2007-4437, 2007.

[21] Kawakami, H., Takatoya, T., and Ishikawa, H., "Static Aeroelastic Analysis of Supersonic Experimental Airplane NEXST-1 Flight Test," AIAA Paper 2007-4174, 2007.

[22] Makino, Y., and Naka, Y., "Sonic-Boom Research and Low-Boom Demonstrator Project in JAXA," 19th International Congress on Acoustics, Madrid, International Commission for Acoustics Paper NLA-08-002-IP, 2007.

[23] Obayashi, S., and Guruswamy, G. P., "Convergence Acceleration of an Aeroelastic Navier–Stokes Solver," *AIAA Journal*, Vol. 33, No. 6, 1994, pp. 1134–1141.

[24] Venkatakrishnan, V., "On the Accuracy of Limiters and Convergence to Steady State Solutions," AIAA Paper 93-0880, 1993.

[25] Sharov, D., and Nakahashi, K., "Reordering of Hybrid Unstructured Grids for Lower-Upper Symmetric Gauss–Seidel Computations," *AIAA Journal*, Vol. 36, No. 3, 1998, pp. 484–486.

[26] Obayashi, S., and Sasaki, D., "Visualization and Data Mining of Pareto Solutions Using Self-Organizing Map," *Evolutionary Multi-Criterion Optimization (EMO 2003)*, Lecture Notes in Computer Science, Vol 2632, Springer–Verlag, Berlin, 2003, pp. 796–809.

[27] Holden, C. M. E., and Keane, A. J., "Visualization Methodologies in Aircraft Design," AIAA Paper 2004-4449, 2004.

[28] Sobol, I. M., "Sensitivity Estimates for Nonlinear Mathematical Models," *Mathematical Modeling and Computational Experiment*, Vol. 1, No. 4, 1993, pp. 407–414.

[29] Jones, D. R., Schonlau, M., and Welch, W. J., "Efficient Global Optimization of Expensive Black-Box Functions," *Journal of Global Optimization*, Vol. 13, No. 4, 1998, pp. 455–492.
doi:10.1023/A:1008306431147

[30] Kohonen, T., *Self-Organizing Maps*, Springer, Berlin, 1995.

[31] Viscovery SOMine, Software Package, Ver. 4.0, Viscovery Software GmbH, Vienna, Austria, 2003.

[32] Vesanto, J., and Alhoniemi, E., "Clustering of the Self-Organizing Map," *IEEE Transactions on Neural Networks*, Vol. 11, No. 3, 2000, pp. 586–600.
doi:10.1109/72.846731